QUANTITATIVE VISUALIZATION OF MIXING IN A MODEL OF AN ARTERIALIZED VEIN PUNCTURED BY A CANNULA

Andreas Borg
Division of Fluid Mechanics
Lund Institute of Technology
Box 118, 221 00 Lund
aborg@ms.vok.lth.se

Laszlo Fuchs
Division of Fluid Mechanics
Lund Institute of Technology
Box 118, 221 00 Lund
Laszlo.Fuchs@vok.lth.se

ABSTRACT

Steady flow and mixing in a model of an "arterialized" vein punctured by a cannula as occur during hemodialysis are investigated *in vitro*. The motivation is that a major cause of vascular access dysfunction is the development of venous stenoses. The interest in mixing of chemical compounds in the dialyzed blood supplied through the cannula is genuine due the clinical impacts of haemodialysis. One is interested also in the mixing of the two streams; namely the untreated blood through the vein and the treated blood through the cannula. This mixing affects the local pH, which in turn can affect the solubility of several salts used for dialysis. This may lead to undesired chemical or bio-chemical processes in the region around the needle.

The mixing of a high Schmidt number substance in the stream entering from the cannula with the base flow in the vein is studied by LIF (Laser Induced Fluorescence). The investigations are performed for a range of typical Reynolds numbers in the cannula and the vein found during hemodialysis.

The study shows complicated mixing patterns around the cannula, and that non-uniformities in the blood persist over long distances for the lower flow rates found *in vivo*. For the higher flow rates, the flow loses its stability and mixing is enhanced. The nature of this instability is shown, and quantitative data of concentration fluctuations are given. If these mixing patterns are of significance for the development of venous stenoses, they should be possible to link them to the development of lesions.

INTRODUCTION

The study of flow in large vessels of the human body is an active area of research. In particular the relationship between arterial diseases like atherosclerosis and fluid mechanics is in focus. The aim of these studies is to establish an explanation to why atherosclerotic lesions occur preferentially at certain locations in the arterial tree. Among the cellular components of the arterial wall, the endothelium has received most of the attention. This seems reasonable due to its strategic location, positioned between the flowing blood and the underlying vessel wall.

Several fluid mechanical parameters have been linked to the selective development of stenoses in the arterial tree. Fry (1968) showed that endothelial cells where permanently damaged if the wall shear stress (steady flow) exceeded 40 Pa. This high shear stress level is not generally present in the healthy arterial system. However, during haemodialysis using an arterio-venous fistula, such shear stress levels do exist, Borg (2000). Caro et al. (1971) associated atherogenesis with disturbed mass transfer at low shear stress regions where the flow is slow and convective mass-transfer is impaired. Ku et al. (1985) showed that plaque formation in the carotid bifurcation correlates well with low but oscillating shear stress. Complementary hypotheses have been provided more recently, which include effects of temporal and spatial gradients in the flow. In particular, large spatial variations of the wall shear stress occur at bends and bifurcation where spatial gradients normally are large. It has been shown that endothelial permeability to macromolecules like albumin depends on the wall shear stress level, Jo et al. (1991) and on the wall shear stress gradient by Phelps and De Paola (2000). High frequency fluctuations in wall shear stress make the wall more distensible, Roach (1972).

During haemodialysis, nearly all of the above factors are present in the neighborhood of the cannula. Depending on the flow-rate in the cannula (speed of dialysis) the flow may be laminar or transitional-turbulent. Regions of elevated wall shear stress (close to 40 Pa) are present on the vein wall around the cannula and on the wall where the cannula jet impacts on the curved vein wall, see Borg (2000). Regions of permanently low shear stress and/or high shear stress gradients exist close to the cannula. For the highest flow rates possible *in*

vivo high frequency oscillations in wall shear stress, and high Reynolds stresses in the interior of the flow exist, see Borg (2000).

Recently, it has been discovered that certain salt precipitations are present in stenotic AV-fistulas (arterio-venous fistulas). These deposits are present only in stenotic AV-fistulas and are absent in non-stenotic fistulas, nor in stenotic lesions that occur at other places in the arterial tree, Olsson (2000).

Here, we report some results that reveal how a possible inhomogeneity in the blood, due to the two streams, from the cannula and the base flow in the vein develops. This concentration inhomogeneity interacts with the above-mentioned factors that may trigger the development of a venous stenosis.

The mixing of a substance that is in excess in the stream from the cannula is studied with LIF (laser induced fluorescence) in an *in vitro* setup. The influence on the mixing patterns of the flow rates in the cannula and the vein, and on the position of the cannula is reported.

METHODS

The experimental setup is aimed to mimic the flow conditions around a real cannula. The geometry is therefore a somewhat simplified up-scaled version of a real cannula.

The real cannula has an inner diameter of 1.8 mm and an outer diameter of 2.0 mm. The veins at the arm after the fistula have a diameter of 2-5 mm but vary greatly from one patient to another. The rig is scaled such that it approximately corresponds to a real vein segment with an inner diameter of 4.3 mm. The angle between the vein and the cannula is fixed to 10°.

Two different positions of the cannula are considered. In the first position, O1, the cannula tip is positioned 1 mm above the vein floor. A schematic picture of the vein and the cannula in position O1 is provided in Fig. 1. In the second position, named O2 the cannula is rotated 180° around its axis compared to configuration O1.

Reference values for the flow rate through the real vein and the cannula are 0.26 l/min and 0.60 l/min respectively. The flow rate through the fistula is then 0.86 l/min (0.26+0.60 l/min). Assuming a viscosity of whole blood of $4x10^{-3}$ kg/sm and a density of 1000 kg/m^3, the bulk Reynolds number in the cannula is 760, 740 in the vein and 1060 in the vein downstream of the cannula. These are reference values and we have varied the flow parameters around these values. The concentration of a substance downstream of the cannula is expected to follow the functional relationship:

$$c = f(x, y, z, D_c, D_v, U_c, U, \alpha, \rho, \mu, D, C_c, C_v)$$

Here, c is the concentration of the substance, x, y, z are the coordinates, D_c is the diameter of the cannula, D_v is the diameter of the vein. U_c is the mean velocity in the cannula, U is the mean velocity in the vein downstream of the cannula. α is the angle between the cannula and the vein, ρ is the density of the fluid, μ is the viscosity of the fluid. D is the diffusivity of the passive scalar, C_c and C_v are the concentrations of the passive scalar in the two streams. Using dimensional analysis with U, ρ, and D_v as the reduction variables the following relation is obtained.

$$c = \Pi\left(\frac{x}{D_v}, \frac{y}{D_v}, \frac{z}{D_v}, \frac{D_c}{D_v}, \mathrm{Re}, \frac{U_c}{U_v}, \alpha, Pe, C_c, C_v\right)$$

where Re is the Reynolds number and Pe is the Peclet number given by:

$$\mathrm{Re} = \frac{UD_v\rho}{\mu}, \quad Pe = \frac{UD_v}{D}$$

Investigated Cases

The following cases are investigated in this paper:

Case	A	B	C
	U_c/U=1.15 U_c/U_v=1.44	U_c/U=1.73 U_c/U_v=2.47	U_c/U=2.30 U_c/U_v=3.84
1	Re=409 Re_c=196 Re_v=327	Re=409 Re_c=295 Re_v=286	Re=409 Re_c=393 Re_v=246
2	Re=818 Re_c=393 Re_v=655	Re=818 Re_c=589 Re_v=573	Re=818 Re_c=786 Re_v=491
3	Re=1310 Re_c=629 Re_v=1048	Re=1310 Re_c=943 Re_v=917	Re=1310 Re_c=1258 Re_v=786
4		Re=1638 Re_c=1179 Re_v=1146	

Table 1: Cases considered in the current study

In table 1 the ratio between mean velocity in the cannula and mean velocity in the vein U_c/U_v is also given .A high value of this ratio implies a more jet like flow.

Experimental Setup

The experimental setup consists of two pumps and two elevated tanks, which provide the necessary head to drive the flow through the model vein and cannula. The model of the vein is made of glass and has an inner diameter of 22 mm. The model of the cannula is made of plexi-glass and has an inner diameter of 9 mm and an outer diameter of 13 mm. The length of the model of the vein is 2,5 m before the cannula is inserted into the stream, which assures a fully developed laminar profile before the insertion point. The length of the cannula is 0.5 m, which also assures a nearly developed flow for the Reynolds numbers considered. The working fluid is water with a temperature of 293° +/- 3° K. To quantify mixing we use Rhodamine B in combination with a pulsed Nd:YAG laser. Rhodamine B is an organic molecule

and has a strong fluorescence centered on the red orange part of the visible spectrum. The maximum absorption of Rhodamine B occurs around 540 nm, which is close to the wavelength of the Nd:YAG laser (532 nm). To reduce refraction index errors the measurement section is submerged in a water-filled plexi-glass box. The imaging system consists of a cross-correlation 1280x1024 pixel CCD-camera (PCO SensiCam Double Shutter) with Nikon Micro-Nikkor 60-mm f/2.8 lenses. The scattered laser light is filtered out using a long pass filter (Kodak Wratten No. 22). A dual head Nd:YAG laser (Continuum Minilite PIV) 0f 2x25 mJ is used for illumination. Light sheet optics forms the laser beam to a sheet. The light sheet is cut by a slit, reducing the laser sheet thickness to 0.5 mm. The timing of the system is controlled by a PC using software from La Vision. The same system has been used for DPIV measurements on this flow.

LIF Measurements

We now describe the procedure used for quantitative concentration measurements. The description here is limited to when the intensity is linearly related to the concentration. A more general description is provided in Van Cruyningen at al. (1990). For fixed optical settings in the linear range the following simplified equation holds for the digital signal level $i_d(x,y,n)$ in each pixel of the camera array for each laser pulse:

$$i_d(x,y,n) = k(x,y,n)c(x,y) + i_{db}(x,y,n) \quad (1)$$

In this equation $k(x,y,n)$ incudes variations in laser energy over the sheet for pulse n and optical factors. $i_{db}(x,y,n)$ is the is the background fluctuations for zero concentration. We introduce the variable $i_{dc} = i_d - i_{db}$, that is the digital signal level with the local background subtracted and the following equation is obtained:

$$i_{dc}(n) = k(n)c \quad (2)$$

were the coordinates have been dropped. We can consider each pixel in the CCD array as the same procedure is applied to all pixels. We assume that fluctuations in laser energy and local background are so small that a reasonable estimate of k can be obtained by averaging over N pulses:

$$I_{dc} = Kc, \text{ or } \frac{1}{N}\sum_{i=1}^{N} i_{dc}(i) = \left(\frac{1}{N}\sum_{i=1}^{N} k(i)\right)c \quad (3)$$

To determine the constant K in each pixel, least square minimzation is done over M tested concentrations in the assumed linear range resulting in the following estimate for K:

$$\hat{K} = \frac{\sum_{i=1}^{M} I_{dc}(i)c(i)}{\sum_{i=1}^{M} c(i)c(i)} \quad (4)$$

Confidence intervals for K, are given by:

$$K = \hat{K} \pm t_{m-2}\frac{s}{\sqrt{\sum_{i=1}^{M}\left(c(i)-\bar{c}\right)^2}}$$
$$s = \sqrt{\frac{1}{M-2}\sum_{i=1}^{M}\left(I_{dc}(i)\right) - Kc(i))^2} \quad (5)$$

In these equations overbar denotes mean value and t_{m-2} is the t-distribution for M samples. With help of this equation the accuracy of the fit can be determined in each point in the pixel array. Typical values for the uncertainty of K is 5% in the current cases. The fluctuations in the background are characterized by the standard deviation computed for 20-30 samples of images with the laser running, but no tracer in the system. In each point we can estimate the total relative uncertainty:

$$\varepsilon_c = \sqrt{(\varepsilon_K)^2 + (\varepsilon_{laser})^2 + (\varepsilon_{bg})^2} \quad (6)$$

where the first parameter under the root is the relative uncertainty in the linear regression, the second is the relative uncertainty due to fluctuations in laser energy and the last is due to fluctuations in the background. The background error determines the lowest concentration that can be measured with any accuracy. Typical values for the error in the current cases are 5% relative error in K, 2.5% error due to laser fluctuations and about 1% error due to background fluctuations. In the measurements presented here the mean relative error in the instantaneous concentration measurement is 6% and the maximum error is 10%. This holds for concentrations down to 6% of the inlet conentration. In regions with very low concentration the relative error increases due to fluctuations in the background but the absolute error remains low.

RESULTS

The results are presented in terms of mixing patterns in Planes 1 and 2 (see Fig. 1) for the two different positions of the cannula O1 and O2. As outlined in Table 1, ten different cases have been investigated. For cases denoted by A, B and C the velocity ratio between the cannula and the vein stream is kept constant. For a specific case number the Reynolds number in the vein downstream of the cannula is kept constant.

We start by looking at results for mixing patterns in Plane 1. In Fig. 2, instantaneous mixing patterns for position O1 of the cannula are shown. The image plane extends from the cannula tip to four diameters downstream of the cannula tip. The pictures show gray scales of normalized concentration. For the cases 1A-1C, the flow and mixing patterns are laminar. We note that the region of high concentration near the vein floor extends over an increased distance when the cannula to vein velocity

ratio increases. This is partly due to an increased momentum of the cannula jet and partly due to weaker compression of the jet by the rotational motion of the flow in the vein induced by the cannula. Numerical simulations of case 1A-2C show that two pairs of counter rotating vortices are set up behind the cannula. The strength of these vortices declines as we change from case A-C. When the Reynolds number is increased to 818 (Fig. 2 Case 2A-2C) the mixing patterns remains approximately the same as for case 1A-1C. We note that in case 2C weak signs of transition are seen in the form of small blobs of high concentration. Similar structures are seen in Case 3A but, in this case, in the interior of the flow field and further downstream. In Case 3B, 3C and 4B the instability appears early in the cannula jet shear layer.

Velocity measurements made by DPIV on Case 4B shows that in this case the wall jet downstream of the cannula has a width that is small compared to the radius of the vein. In the region where it starts to interact with the lower vein wall, we can consider it as approximately plane. Furthermore, the jet transverse velocity in this region is small although it increases quite fast as we move away from the wall region. We have calculated the second derivative of the axial velocity in the transverse direction for this case, which shows that the jet profile has an inflection point. Around one vein diameter downstream of the cannula tip the upper side of the wall jet is well approximated by $u=a+b/\cosh^2(y-y_{0/}\delta)$ where y_0 is the center of the plane jet. The shear layer width is $\delta=0.05\ D_v$ at this position and the distance between the vortices leading to the mixing patterns in Case 4B is 6δ. This is fairly close to the wavelength of the mode with maximum amplification rate for a high Reynolds number Bickley jet [$u=b/\cosh^2(y-y_{0/}\delta)$] given by Lesieur (1997) which is $6.55\ \delta$.

In Fig. 3, the corresponding mixing patterns for the case when the cannula is rotated around its axis are depicted (position O2). The secondary flow induced behind the cannula is weaker in this case than for position O1. Therefore, the jet is less compressed compared to position O1. As for position O1 Case 1A, B and C remains laminar. In addition, signs of transition are seen in Case 2C and more expressed in 3A-3C.

In Fig. 4, the corresponding fields of the rms of the concentration fluctuations in Plane 1 are depicted. The figures to the left correspond to position O1 of the cannula and the ones to the right to position O2. These figures quantify what is seen in the instantaneous pictures i.e. that fluctuations are nearly absent in Cases 2A and 2B, weak in Case 2C and significant in Cases 3A, 3B and 3C. Note the fast growth of instabilities in the jet shear layer in Case 3C which leads to strongly enhanced mixing further downstream and high levels of concentration fluctuations close to the lower vein wall in the studied domain.

Instantaneous mixing patterns in Plane 2 for position O1 of the cannula are presented in Fig. 5. The images depict the plane from the cannula tip to 3.2 diameters downstream of this position. The general behavior of the flow field is governed by the cannula jet that hits the lower vein wall and spreads along the vein wall, and the secondary flow induced by the jet. This leads to complicated mixing patterns even in the laminar cases, which consist of long tiny structures of high concentration. We note that high concentration regions exist close to the vein walls for long distances downstream of the cannula in this plane. The formations of the patterns in Fig. 5 are easier to understand with support from Fig. 6. This figure shows the mixing patterns in different cross-sections of the vein taken from numerical simulations for Case 1A and 1C. In this figure, we clearly see how the flow from the cannula hits the vein wall and spreads up along the vein walls as we move downstream. For the higher Reynolds number cases we see that the elongated structures breaks down and small scale mixing is visible, see Fig. 5. Fig. 5 is complemented with Fig. 7, which shows the rms of the concentration fluctuations on Plane 2. For the Cases 2A-2C fluctuations are weak in this plane and for case 3A and 3B, fluctuations appear in narrow bands around the structures seen in Fig. 5. We see that in case 3C the concentration fluctuations are large in regions close to the vein wall and get more uniformly distributed in the plane as we move downstream of the cannula tip.

CONCLUDING REMARKS

The mixing around a model of a cannula puncturing a vein during hemodialysis have been studies for physiological flow rates. The flow parameters are varied so that they correspond to different flow rates through the fistula and different speeds of the dialysis.

The results show that the flow changes from laminar to transitional depending of these two parameters. The impact of this on the mixing patterns and the rms of the concentration fluctuations in the neighborhood of the cannula are shown.

In the laminar cases, the concentration of the substance entering from the cannula remains high along parts of the vein wall for long distances downstream. For the higher Reynolds numbers the flow lose stability leading to high frequency concentration fluctuations [$O(10^2)$-$O(10^3)$ Hz] close to the wall in the real application. The rms values of the concentration fluctuations close to the vein wall are high in those cases.

It remains to be seen if these mixing patterns of a substance in excess in the cannula stream can be linked to the locations where venous stenoses develops.

References

Borg, A., 2000, "Experimental and numerical studies of flows related to the processes of atherosclerosis", PhD thesis, Lund Institute of Technology, Sweden.

Caro, C.G., Fitzgerald, J. M., Shroter, R.C. 1971, "Atheroma and arterial wall shear observations, correlation and proposal of a shear dependent mass transfer mechanism for atherogenesis", Proc. R. Soc. London Sr. B, 17(7), pp109-159

Fry, D.L. 1968, "Acute vascular endothelial changes associated with increased blood velocity gradients", Circ. Res., 22, pp. 165-197

Jo, H., Dull, R.O., Hollis, T. M., Tarbell, J. M. 1991 "Endothelial albumin permeability is shear dependent, time dependent, and reversible", Am. J. Physiol., 269, H1992-H1996

Ku, D. N., Giddens, D. P., Zarins, K. Z. and Glagov, S., "Pulsatile flow and atherosclerosis in the human carotid bifurcation: positive correlation between plaque location and low and oscillating shear stress", Atherosclerosis, 5, pp. 293-302

Lesieur, M. 1997, "Turbulence in fluids", Kluwer Academic Publishers

Olsson, Lars-Fride 2000, Private Communication in Aug. 2000, Gambro Research, Gambro AB, Lund, Sweden

Phelps, J. E., DePaola, N. 2000 "Spatial variations in endothelial barrier function in disturbed flow in vitro", Am. J. Physiol., 278, H469-H476

Roach, M. R. 1963 "An experimental study of the production and time course of poststenotic dilation in the femoral and carotid arteries of adult dogs", Circ. Res., 13, pp. 537-551

Van Cruyningen, I., Lazano, A., Hanson, R.K. 1990 "Quantitative imaging of concentration by planar laser-induced fluorescence, Exp. in Fluids, 10, pp. 41-49

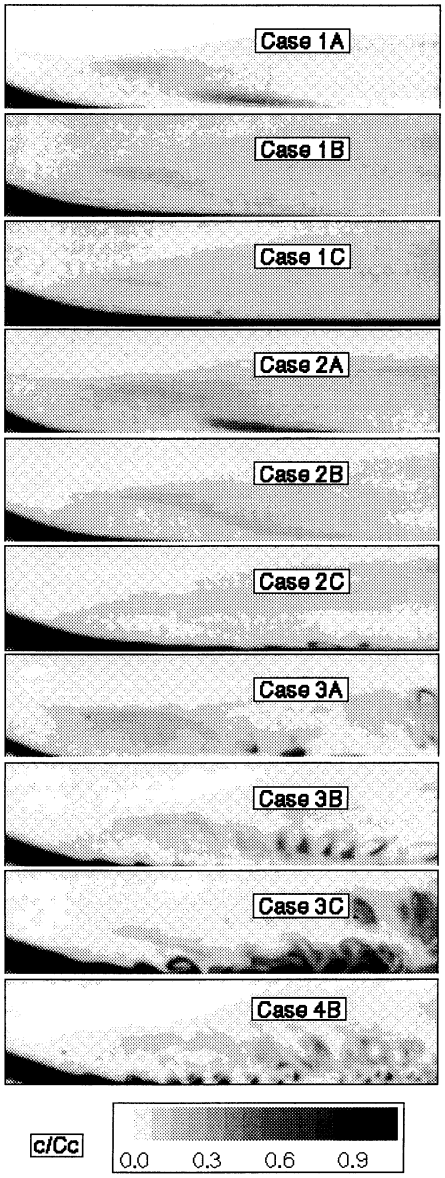

Fig. 2 Instantaneous mixing patterns in plane 1 for position O1 of the cannula. The legend shows the level of c/C_c

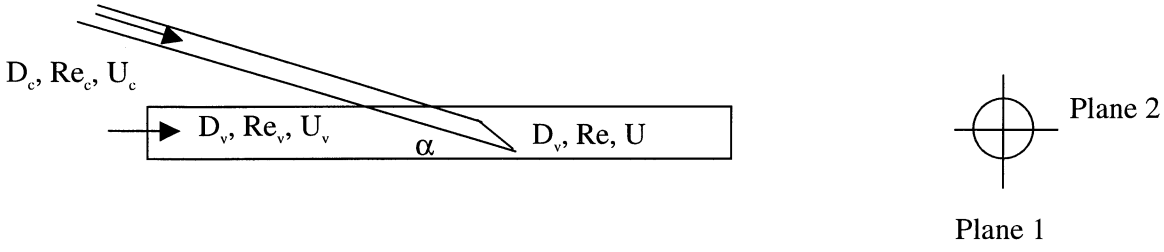

Fig. 1 Schematic picture of the cannula puncturing the vein.

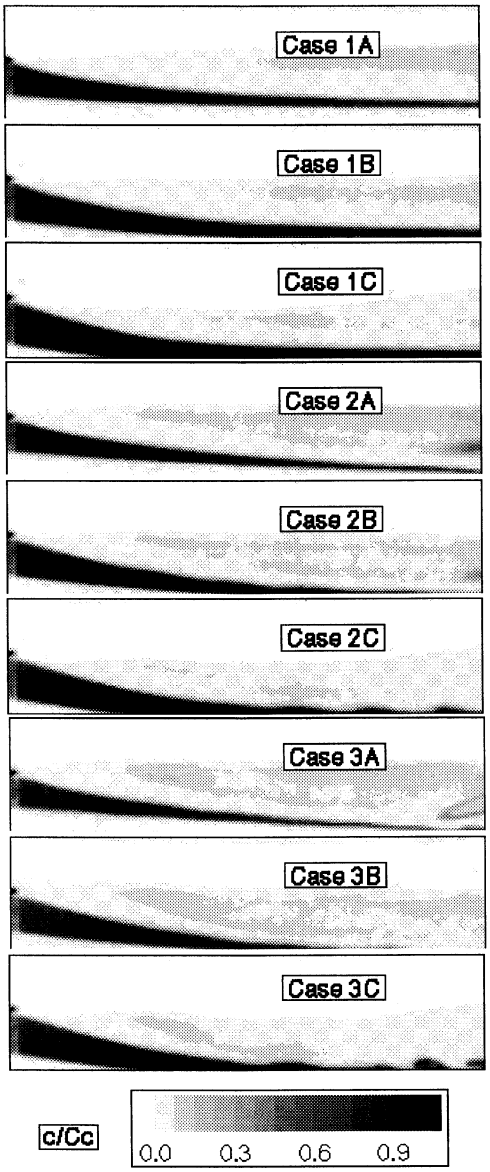

Fig. 3 Instantaneous mixing patterns in plane 1 for position O2 of the cannula.

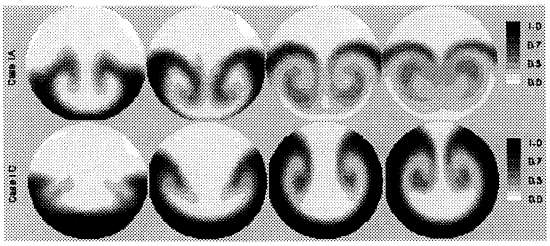

Fig. 6 Mixing patterns downstream of the cannula tip. Cannula position O1. The position of the cross-sections are from left to right at x/D_v=1, 2, 4 and 6, where x is the coordinate from the cannula tip. The legend shows the level of c/C_c.

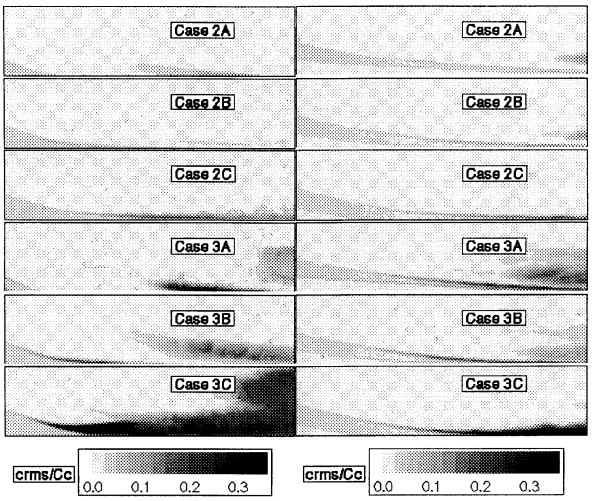

Fig. 4 Concentration fluctuations in plane 1. Position O1 of the cannula to the left and position O2 to the right. The legend shows the level of c_{rms}/C_c.

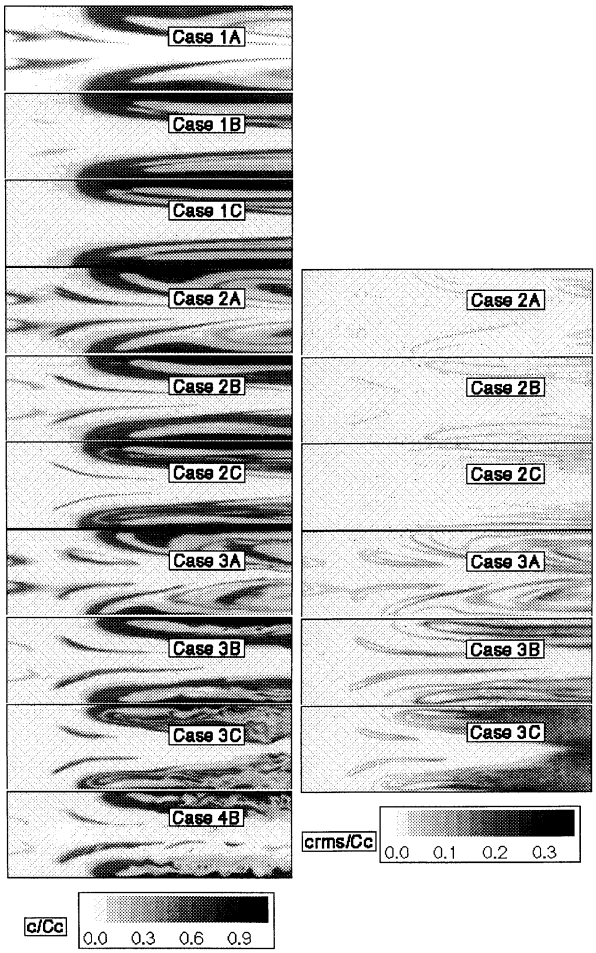

Fig. 5 to the left and Fig. 7 to the right. Fig. 5 shows the mixing patterns in plane 2 for position O1 of the cannula. Fig. 7 shows the corresponding rms fields of concentration fluctuations for case 2A-3C.